

Deceiving Flexibility: A Stealthy False Data Injection Model in Vehicle-to-Grid Coordination

Kaan T. Gun; Xiaozhe Wang

*Department of Electrical and Computer Engineering
McGill University*

Danial Jafarigiv

L'Institut de recherche d'Hydro-Québec (IREQ)

Abstract—Electric vehicles (EVs) in Vehicle-to-Grid (V2G) systems act as distributed energy resources that support grid stability. Centralized coordination such as the extended State Space Model (eSSM) enhances scalability and estimation efficiency but may introduce new cyber-attack surfaces. This paper presents a stealthy False Data Injection Attack (FDIA) targeting eSSM-based V2G coordination. Unlike prior studies that assume attackers can disrupt physical charging or discharging processes, we consider an adversary who compromises only a subset of EVs, and limiting their influence to the manipulation of reported State of Charge (SoC) and power measurements. By doing so, the attacker can deceive the operator's perception of fleet flexibility while remaining consistent with model-based expectations, thus evading anomaly detection. Numerical simulations show that the proposed stealthy FDIA can deteriorate grid frequency stability even without direct access to control infrastructure. These findings highlight the need for enhanced detection and mitigation mechanisms tailored to aggregated V2G frameworks.

Index terms— Cyberattack, False Data Injection Attacks, Electric Vehicles, State Space Model, Vehicle-to-Grid

I. INTRODUCTION

Electric vehicles (EVs) are gaining attention as governments worldwide implement supportive policies and invest in green technologies to achieve emission reduction goals [1]. One promising advancement in this domain is Vehicle-to-Grid (V2G) technology, which enables bidirectional energy flow between EVs and the power grid, allowing EVs to act as distributed energy resources (DERs) that enhance grid stability [2] and facilitate the integration of renewable energy [3]–[6].

However, challenges persist due to the uncertainty of travel patterns, diverse charging behaviors, and the complexity of managing large EV fleets. In V2G frameworks, centralized algorithms have been proposed where a central operator coordinates EV charging to support the grid and optimize fleet performance [7], [8]. A key challenge with such approaches is scalability; as the number of EVs grows, the communication cost and computational burden associated with collecting frequent state updates (like State-of-Charge (SoC)) from each vehicle increase significantly [9]. To address this limitation, the State Space Model (SSM) was introduced [10] and further extended in [11]. Given that V2G systems rely on sophisticated communication and control, research into the cybersecurity vulnerabilities of charging infrastructure has intensified in [12] to ensure the reliability and safety of grid operations.

Previous cybersecurity studies have explored threat assessments on spoofing, tampering, and Distributed Denial-

of-Service (DDoS) in EV chargers [13], [14]; similarly, in the context of smart charging management systems [15], [16] others have investigated designing attack vectors targeting individual EV charging sessions that could potentially cause physical damage to vehicle batteries [17]. Furthermore, the integration of EVs as cyber-physical assets has prompted investigations into grid stability under large-scale load manipulation attacks [18], often assuming the attacker gains significant or full control over charging assets.

However, when considering attacks within an actively managed V2G framework, the presence of a central coordinator changes the landscape. Such coordinators typically employ operational models to predict and manage the fleet's aggregated behavior for grid services. Consequently, overt or large-magnitude brute-force attacks, which would cause significant discrepancies between the measurements and the values expected by the operator's model, are likely to be rapidly identified through anomaly detection mechanisms. In contrast to prior works [12], [16]–[18], which often assume direct attacker control over individual chargers or EVs, or do not explicitly account for the monitoring capabilities inherent in centralized V2G coordination, we consider a more nuanced scenario. Our model assumes the fleet operator employs the extended State Space Model (eSSM) as a centralized V2G control strategy [10], [11], while the attacker has limited knowledge and lacks direct control over the charging infrastructure, necessitating more sophisticated or stealthy approaches to impact the system effectively.

Such strategy allows for monitoring and controlling the charging dynamics of the fleet, leveraging the eSSM's recognized advantages in scalability, communication efficiency, and state estimation, which enhances the situational awareness [10], [11]. While eSSM-based control inherently offers some resilience against certain threats due to reduced communication needs and aggregated modeling, possibilities remain for constructing sophisticated cyberattacks. In this work, we specifically analyze a scenario under the realistic assumption that attacker cannot directly compromise the V2G framework or alter the control signals dispatched to individual EVs or chargers. We propose a stealthy Man-in-the-Middle (MitM) False Data Injection Attack (FDIA) model targeting the eSSM-based V2G system. This attack involves compromising a subset of participating EV manufacturers' backend communication and manipulating their reported data with the aim of misleading the operator's state estimation and control logic. We demonstrate that even without accessing the charger or EV infrastructure, an attacker can exploit local information

This work was supported in part by the Fonds de recherche du Québec-secteur Nature et technologies (FRQ-Secteur NT) under Grant 2023-NOVA-314338 and in part by the Hydro-Québec, the Institut de Valorisation des Données (IVADO), MITACS under Grant IT27493.

to coordinate the injection of false data stealthily, thereby avoiding straightforward detection by the central coordinator's anomaly detection mechanisms. The potential consequence of such a successful stealthy attack is the degradation of grid services, possibly leading to operational inefficiencies, financial losses, or impacting grid frequency.

II. PRELIMINARIES

This section introduces the individual and aggregated EV model, detailing their SoC dynamics. A key advantage of the eSSM is that it scales efficiently with the number of vehicles, as its computational complexity is independent of fleet size and instead depends solely on the granularity of the discrete SoC levels. It also addresses communication bottlenecks by broadcasting a unified control signal while requiring EVs to send less frequent but periodic measurements. Thus, the operator utilizes its model to infer the aggregated state and power flexibility of fleets, enabling the utility to dispatch power within the bounds of the fleets' capabilities. Its high accuracy, computational efficiency, and reduced communication overhead make the eSSM highly suitable for managing large-scale EV fleets in grid services.

A. Individual Electric Vehicle Model (IEVM)

An individual EV (i) operates within a well-defined set of parameters (charge start and finish times ($t_{s,i}, t_{f,i}$), start and departure SoC ($S_{s,i}, S_{d,i}$), and SoC range (S_{min}, S_{max})) when connected to a charging station. The fleet operator maintains additional key characteristics such as battery capacity Q_i , and power limits $P_i \in \{P_{c,i}, P_{d,i}\}$, along with the efficiency (η_i).

There are three operating modes for an EV: Charging Mode (CM), where it draws power from the grid to increase its SoC; Idle Mode (IM), where it remains connected but does not exchange power; or Discharging Mode (DM), where it delivers power back to the grid. For the EV index (i), the SoC dynamics can be expressed in discrete time, where its SoC transitions depend on the power exchange with the grid. Mathematically, the SoC at time step $k+1$ is determined as;

$$S_i(k+1) = \begin{cases} S_i(k) - P_i(k) \cdot \eta_i \cdot \frac{T}{Q_i}, & P_i(k) < 0, \text{CM} \\ S_i(k), & P_i(k) = 0, \text{IM} \\ S_i(k) - \frac{P_i(k)}{\eta_i} \cdot \frac{T}{Q_i}, & P_i(k) > 0, \text{DM} \end{cases} \quad (1)$$

The simulation time index is expressed as k . This ensures the feasible operational region of an EV is constrained by its SoC and power limits, and the battery remains within its predefined charge boundaries.

B. The Extended State Space Model of Aggregated EVs

The State Space Model (SSM) represents the fleets distribution across discrete states (i.e. the proportion of EVs located in the corresponding SoC intervals across operation modes) $\mathbf{x} \in \mathbb{R}^{3N_s}$. For each operation mode (CM, IM, DM), the SoC range [S_{min}, S_{max}] is partitioned into number of discrete SoC intervals N_s . All connected EVs are represented at an index of the aggregated state \mathbf{x} according to their power and SoC measurements. This formulation enables the development of a Markov Transition Model (MTM) $\mathbf{A} \in \mathbb{R}^{(3N_s, 3N_s)}$, which describes the dynamic evolution of the aggregated EV population. Consequently, the state distribution at the next time

step is expressed as $\mathbf{x}(k+1) = \mathbf{A}\mathbf{x}(k)$. It is assumed that EVs are uniformly distributed within each state interval [19].

Beyond the standard operational states, additional conditions affect the ability of EVs to provide grid flexibility. Specifically, when a vehicle reaches its SoC limits ($S_{max,i}, S_{min,i}$), its ability to contribute to charging or discharging services becomes asymmetric. The extended State Space Model (eSSM) captures this effect by introducing additional *Special States* indexes $SS_{MAX} = 3N_s + 1$ and $SS_{MIN} = 3N_s + 3$ [11]. Furthermore, EVs that require immediate charging to meet their departure SoC target transition into a Forced Charging State index ($FCS = 3N_s + 2$), effectively removing them from grid participation.

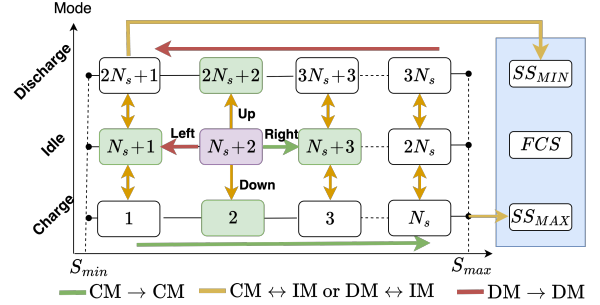


Fig. 1: Illustration of State Indexes and Transitions.

By incorporating these special state indexes, \mathbf{x} expands to a dimension of $3N_s + 3$, and $\mathbf{A} \in \mathbb{R}^{(3N_s+3, 3N_s+3)}$. As represented in Fig. 1, this extended formulation ensures that the eSSM accurately represents the dynamic state distribution of the fleet while accounting for constraints that impact grid flexibility.

The aggregated power output $y(k)$ is calculated based on the distribution $\mathbf{x}(k)$:

$$y(k) = P_{ave}(k) \mathcal{N}(k) \cdot \mathbf{D} \cdot \mathbf{x}(k) \quad (2)$$

where $\mathbf{D} = [-\mathbf{1}_{1 \times N_s} \quad \mathbf{0}_{1 \times N_s} \quad \mathbf{1}_{1 \times N_s} \quad 0 \quad -1 \quad 0]^T$ and P_{ave} is the statistical expectation of the charging powers P_c of the number of all connected EVs $\mathcal{N}(k)$, which can be calculated as $P_{ave} = \int_{P_{c,min}}^{P_{c,max}} P_c f_c(P_c) dP_c$, where $P_{c,min}, P_{c,max}$ are the bounds of is the probability density function (PDF) $f_c(P_c)$.

The PDF characterizes the diversity of charging power ratings within the population. Because the fleet composition is dynamic, the PDF varies over time as the connection states of individual EVs change. By leveraging real-time data points from connected vehicles, the operator recalculates $f_c(P_c)$ at each control interval T_p , thereby providing a more precise P_{ave} estimate for the aggregated power calculation in (2).

Fig. 2 describes the operational flow of the V2G framework, which proceeds in the following steps:

- 1) **Data Transmission:** Once an EV connects to a charger, it transmits user-defined constraints (t_s, t_f, S_c, S_d) and current measurements ($S(k), P(k)$) to the system operator. Subsequently, these measurements are updated every T_p interval.
- 2) **Model Construction:** The operator uses the aggregated data from all vehicles to construct an eSSM.
- 3) **Flexibility Reporting:** The eSSM estimates the total available grid flexibility and sends its upper and lower bounds to the utility.

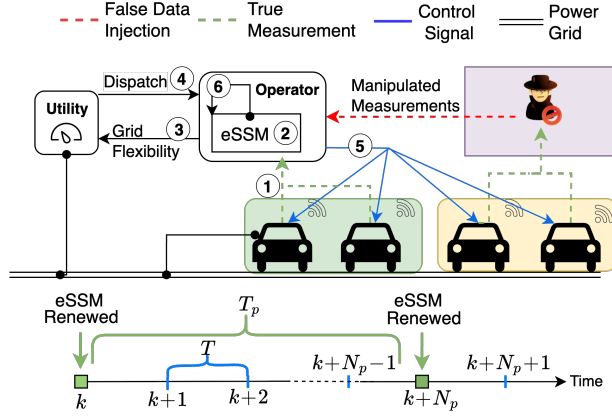


Fig. 2: Overview of V2G Communication and eSSM execution timeline

- 4) **Power Dispatch:** In response, the utility dispatches a power setpoint to the operator.
- 5) **Model Update:** The eSSM computes feedback control signals and updates the eSSM to estimate its state at the next interval $(k + 1)$ to maintain model accuracy.
- 6) **Control Command Broadcasting:** The feedback control signals (\mathbf{u}, \mathbf{v}) are broadcasted to all EVs.

It is assumed that the operator has a prior knowledge of all vehicle specifications $(Q, S_{min}, S_{max}, P_{min}, P_{max}, \eta)$, which remain constant. As depicted in Fig. 2, the eSSM updates its internal state at each time step k over a horizon of T intervals. The model is considered *stale* after it has been updated N_p times, at which point it is renewed with the most recent EV measurements. Thus, eSSM is renewed every $T_p = TN_p$ interval.

The upper and lower boundaries of the fleets grid flexibility is denoted as $y_u(k)$ and $y_l(k)$ is calculated based on $\mathbf{x}(k)$, respectively:

$$\begin{aligned} y_u(k) &= P_{ave}(k) \mathcal{N}(k) \cdot \mathbf{D}_u \cdot \mathbf{x}(k), \\ y_l(k) &= P_{ave}(k) \mathcal{N}(k) \cdot \mathbf{D}_l \cdot \mathbf{x}(k), \end{aligned} \quad (3)$$

where $\mathbf{D}_u = [\mathbf{O}_{1 \times N_s} \quad \mathbf{1}_{1 \times N_s} \quad \mathbf{2}_{1 \times N_s} \quad 0 \quad 0 \quad 2]^T$, $\mathbf{D}_l = [\mathbf{2}_{1 \times N_s} \quad \mathbf{1}_{1 \times N_s} \quad \mathbf{O}_{1 \times N_s} \quad 2 \quad 0 \quad 0]^T$

To effectively regulate the participation of EVs in grid services, a feedback control mechanism is integrated into the eSSM. The feedback signal governs EV transitions between operating modes in response to external grid conditions. This ensures that the aggregated EV population dynamically adjusts its charging behavior while maintaining system stability.

The feedback signal, denoted as $\mathbf{u}(k), \mathbf{v}(k) \in [-1, 1]^{N_s+3}$ are introduced (4) to influence the state distribution at each time step.

$$\mathbf{x}(k+1) = \mathbf{A}\mathbf{x}(k) + \mathbf{B}\mathbf{u}(k) + \mathbf{C}\mathbf{v}(k), \quad (4)$$

where $\mathbf{B} = [-\mathbf{I}_{N_s \times N_s} \quad \mathbf{I}_{N_s \times N_s} \quad \mathbf{O}_{N_s \times N_s}]^T$, $\mathbf{C} = [\mathbf{O}_{N_s \times N_s} \quad -\mathbf{I}_{N_s \times N_s} \quad \mathbf{I}_{N_s \times N_s}]^T$ excluding the special states, are the constant matrices that determines how the feedback signal modifies the state transitions across different SoC intervals.

$\mathbf{u}(k), \mathbf{v}(k)$ vectors are derived based on $\mathbf{x}(k)$ and designed to enforce grid-supporting behaviors while respecting individual EV directives. If the total power requested by the utility ΔP_r is within the bounds of grid flexibility, the

operator constructs the feedback signals based on a state-based priority function $\rho(\mathbf{x}(k), \mathcal{N}, P_{ave})$. e.g. when power reduction is requested, EVs that are in CM and have high-SoC values are prioritized for switching to IM.

Finally, $\mathbf{u}(k), \mathbf{v}(k)$ are mapped to control signals \mathbf{u}_s and \mathbf{v}_s that consist of two probabilistic vectors $[0, 1]^{N_s}$, along with a Control Direction Element $\text{CDE} \in \{-1, 1\}$, instructing EVs on whether to transition between operating modes in response to grid requirements. Each EV autonomously determines whether to execute the requested transition based on where it locates in the state space (see Fig. 1).

$$\mathbf{u}_s : \begin{cases} \text{CM} \rightarrow \text{IM} & \text{if CDE}+ \\ \text{CM} \leftarrow \text{IM} & \text{if CDE}- \end{cases} \quad \mathbf{v}_s : \begin{cases} \text{IM} \rightarrow \text{DM} & \text{if CDE}+ \\ \text{IM} \leftarrow \text{DM} & \text{if CDE}- \end{cases} \quad (5)$$

These control signals represents the probability distribution of switching at each state index, and are then broadcast to all EVs. Since individual vehicles know their current state index, corresponding vehicle switch their operation modes, resulting the aggregated change in power flow $\Delta P_{EV} \approx \Delta P_r$ [10]. This approach eliminates the need for the operator to generate individual control signals for each vehicle.

III. THE PROPOSED STEALTHY FDIA MODEL

We assume an attacker performs a MitM-FDIA by compromising a random subset of vehicles. As depicted in Fig. 2, the attack targets the vehicle-to-operator measurement pathway by accessing backend servers of certain EV manufacturers. This allows the adversary to manipulate the SoC and power measurements from compromised EVs over time, after the initial transmission. The attacker has no control over the physical charging process itself, unable to vary power levels, physically disconnect EVs, or alter the true energy stored in the battery. Its objective is to deviate operators view of the estimated grid flexibility from true flexibility.

A. Stealthy Conditions

Since the state distribution \mathbf{x} is estimated using eSSM over a period T_p , both \mathbf{x} and \mathbf{A} are updated based on the most recent EV measurements. Let $\mathbf{x}_{\text{eSSM est.}}(k)$ denote the last estimated state at the end of T_p by the eSSM (i.e., the stale state distribution). When the eSSM is updated with new, real-time EV measurements, its accuracy dictates that the new state vector $\mathbf{x}_{\text{true}}(k)$ should closely align with the prior estimate. Therefore, to ensure stealthy conditions, the eSSM's estimates derived from manipulated measurements must closely approximate those based on real-time measurements.

$$|\mathbf{x}_{\text{true}}(k) - \mathbf{x}_{\text{eSSM est.}}(k)| < \epsilon, \quad \text{when } \text{mod}(k, N_p) = 0 \quad (6)$$

The aggregate stealth bound in (6) limits large deviations in the fleet's state vector. However, since the operator receives measurements from individual EVs, the reported values must also respect each EV's SoC and power constraints over the period T_p :

$$P_{d,i} T_p \leq Q_i \cdot \text{sgn}(\Delta S_i) |\Delta S_i| \leq P_{c,i} T_p \quad (7)$$

$$P_{d,i} \leq P'_i \leq P_{c,i} \quad (8)$$

where $\Delta S_i = S'_i - S_i$ is the change in SoC for EV i and determined by the successive measurements denoted as (S'_i, P'_i) . Round away from zero is used due to limited granularity of reported SoC ($G_{SoC} = \%1$).

B. Multi-Stage FDI Attack

The attacker optimizes its FDIA strategy by exploiting the dynamics of the eSSM. To remain undetected, the attacker ensures that both the previously transmitted individual EV measurements, and the newly manipulated measurements, satisfy the stealthy constraints defined in (7) and (8). The attack optimization is executed at the same frequency, i.e., every T_p , as the EV measurement transmission frequency. The FDI Attack procedure is described in Fig. 3 and each step is explained accordingly.

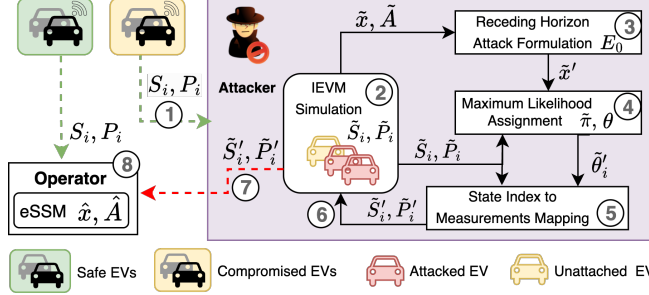


Fig. 3: FDI Attack Procedure Green and red dashed lines indicate the true and manipulated EV measurements respectively.

1) **Collection of compromised EV measurements:** The attack starts when enough vehicles are anticipated to connect to chargers. Once begins, the attacker uses the compromised EV measurements S_i and P_i to build its IEVM simulation. Since the EVs send updated measurements every T_p period, attacker updates its simulation with the *true* measurements of *un-attacked* EVs and adds newly connected vehicles.

2) **IEVM Simulation:** The attacker has access to a subset of the fleet, which consists of the compromised EVs. The primary purpose of the IEVM (section II-A) is to emulate the dynamics of individual EVs using manipulated measurements, and it supplies these false measurements to the operator. The attacker then uses these emulated EV measurements to derive the necessary parameters for subsequent steps of the attack. As the attack progresses, the IEVMs of the targeted EVs are updated with manipulated measurements ($\tilde{S}'_i, \tilde{P}'_i$). In this notation, the tilde symbol ($\tilde{\square}$) indicates the value that is the output of the IEVM simulation, while the prime symbol (\square') indicates the manipulated value. The combination of both symbols ($\tilde{\square}'$) indicates that the measurements are sampled from the IEVM simulation, manipulated by the attacker, and then sent to the operator.

At each measurement interval T_p , simulated IEVM measurements are employed to construct the aggregated state and the transition matrix ($\tilde{x}(k)$ and $\tilde{A}(k)$) for the compromised vehicle subset, thereby emulating the eSSM parameters in the operator room. Furthermore, simulation is also utilized to determine each vehicle's state indices and their state transition weights, $\tilde{\pi}_i(k)$ using the Algorithm 1 to map the manipulated aggregated state distribution $\tilde{x}'(k)$ back to individual EV measurements $\tilde{S}'_i, \tilde{P}'_i$. Details will be found in III-B4.

3) **Receding Horizon Attack Formulation:** In the first stage of the attack, $\tilde{x}(k)$ and $\tilde{A}(k)$ are used to determine the aggregated attack vector \tilde{x}' . As shown in Fig. 4, this stage is formulated as a multi-period optimization problem designed to find an optimal initial manipulation matrix, E_0 (9). A receding

horizon control strategy is employed where a long-term plan is formulated to inform an immediate, optimal deviation of the aggregate state vector. The attack is optimized at the current time index k and planned over an optimization horizon (T_H).

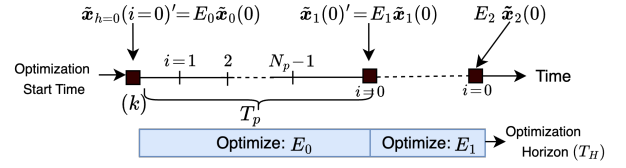


Fig. 4: Illustration of the optimizations cascading timeline. Output of the IEVM $\tilde{x}_0(0)' = E_0 \tilde{x}_0(0)$. At the end of period h , the manipulated state evolved under SSM becomes the initial state for the next period $h+1$.

Thus, problem is formulated to find the sequence of matrices $\{E_0, \dots, E_{T_H}\}$ that maximizes the cumulative flexibility deviation over the entire planning horizon:

$$\max_{E_0, \dots, E_{T_H}} \sum_{h=0}^{T_H} \sum_{i=0}^{N_p-1} [D_i \tilde{x}'_h(i) - D_i \tilde{x}_h(i)] \quad (9)$$

where $\tilde{x}'_h(i) = \tilde{A}_h^i E_h \tilde{x}_h(0)$ is the state under manipulation, $\tilde{x}_h(i) = \tilde{A}_h^i \tilde{x}_h(0)$ is the state estimate without manipulation, that can be calculated from the output of IEVM.

The optimization is subject to:

a) **Aggregate Stealth Constraint:** According to the stealth constraint (10), to remain undetected, the deviation between the manipulated and reference state distributions at the start of each period must be bounded by a threshold ϵ .

$$\|E_h \tilde{x}_h(0) - \tilde{x}_h(0)\| \leq \epsilon \quad h \in \{0, \dots, T_H\} \quad (10)$$

where $E_h \tilde{x}_h(0)$ represents the manipulated state distribution and $\tilde{x}_h(0)$ the output of the IEVM, emulating part of the observation at the operator room.

b) **Individual Physical Feasibility:** The manipulation must respect the physical constraints of individual EVs. The aggregate manipulation matrix E_h must only represent state transitions that are feasible over a period T_p (as shown in Fig. 1). Thus, the elements of the manipulation matrix is constrained as:

$$(E_h)_{mn} \begin{cases} \in [0, 1] & \text{if } (m, n) \in \phi \\ = 0 & \text{otherwise} \end{cases} \quad h \in \{0, \dots, T_H\} \quad (11)$$

where ϕ is the set of allowed transitions between states that satisfy individual EV power and energy constraints over the interval T_p . For example, if we consider state index $m = 15$ (representing a SoC block of 40-49% in the idle mode), it can only transition to idle, charging, and discharging modes within the same SoC block in T_p period. Therefore, the allowed transitions for $m = 15$ are $n \in \{5, 15, 25\}$, meaning state indexes (15,5), (15,15), and (15,25) of ϕ could be assigned a value between $[0, 1]$.

c) **Conservation Constraint:** After state manipulation, the aggregate distribution of fleet across the state indexes must be equal to 1.

$$\sum E_h x_h = 1 \quad (12)$$

Although the optimization in (9) is solved for the entire horizon, only the initial matrix E_0 is implemented to generate the attack vector for the current interval:

$$\tilde{x}'(k) = E_0 \tilde{x}_0(k) \quad (13)$$

TABLE I: Fleet Parameters

Parameter	Description	Value*
S_s	Start Charging SOC	$N(0.2, 0.05) \in [0.2, 0.4]$
S_d	Demanded SOC for Travel	$N(0.85, 0.03) \in [0.75, 0.95]$
t_s	Start Charging Time (h)	$N(-6.5, 3.4) \in [0, 5.5]$
t_f	Finish Charging Time (h)	$N(8.9, 3.4) \in [0, 20.9]$
S_{min}/S_{max}	Minimum/Maximum SOC Value	0.05/0.95
P_c/P_d	Charging/Discharging Power (kW)	U(6.0, 8.0)
η	Charging/Discharging Efficiency	U(0.88, 0.95)
Q	Battery Capacity (kWh)	U(20.0, 40.0)
T_p	Optimization Period	5 min.
T	Optimization interval count	20 sec.
ϵ	Aggregated State Distribution Error	0.01
T_H	Optimization horizon	2
N_p	Optimization interval count	5

$U(a, b)$ denotes a uniform distribution with variation range $[a, b]$.

$N(\mu, \delta)$ denotes a normal distribution where μ is the mean value and δ is the standard deviation. $[a, b]$ is the variation range.

This is because multi-period optimization functions as a planning mechanism to determine the optimal initial manipulation (E_0) by forecasting its cascading effects over future periods.

4) **Maximum Likelihood Assignment:** Once the aggregate state distribution $\tilde{\mathbf{x}}'(k)$ is optimized, it must be mapped to the measurements of individual EV, as the operator receives distinct measurements from each EV rather than a single aggregate value. This second stage of the optimization performs this mapping by assigning a specific target state to each compromised vehicle using a Maximum Likelihood Estimation (MLE) approach.

Here, the attacker's goal is to choose which vehicles' reported values to alter so the manipulated aggregate $\tilde{\mathbf{x}}'$ can be reconstructed by the operator while satisfying the physical constraints (7), and (8). For example, an EV with 51% SOC in charging mode is unlikely—given the physical power limits in (7) and (8)—to reach the 60–69% SOC interval within T_p interval, while an EV currently at 59% SOC in charging mode could plausibly shift into the 60–69% interval. To capture these practical transition probabilities, a weight vector $\tilde{\pi}_i$ (see Algorithm 1 in Appendix) is computed for each EV i . $\tilde{\pi}_i$ quantifies the attacker's probabilistic assessment of the vehicle's state transitions according to their operating mode and SoC level. This vector is formulated as a composite of two distinct weight vectors:

a) **State Transition Across Operating Modes:** These model the likelihood of vehicle changing operating modes. EVs with higher SoC while in Charging Mode (CM) are assigned larger weights for transitioning to Idle Mode (IM), which facilitates CM \rightarrow IM. Conversely, vehicles with lower SoC are assigned higher weights for following the DM \rightarrow IM \rightarrow CM sequence.

b) **State Transition Within an Operating Mode:** These capture the probability of advancing within the same operating mode to the next SoC interval. An EV in CM with a high local SoC position receives greater weight for moving to the next SoC interval. Conversely, IM or DM with low SoC position receives greater weight for moving to the previous SoC interval.

The attacker's objective is to determine the optimal state transition for each compromised EV, leveraging $\tilde{\pi}_{i \dots N_{comp}}$ to guide strategic switching decisions. Thus, formulating a mixed integer linear programming problem where the decision variables $\theta_{i,j} \forall j \in 3N_s$ (excluding special states) represent the state index transitions for each EV.

$$\max_{\theta} \sum_{i=1}^{N_{comp}} \sum_{j=1}^{3N_s} \theta_{ij} \log(\tilde{\pi}_i(j | S, P)) \quad (14)$$

subject to:

$$\theta_{ij} = 0 \quad \forall i \in \mathcal{N}_{comp} \quad \forall \tilde{\pi}_i(j | S, P) \leq 0$$

$$\sum_{j=1}^{3N_s} \theta_{ij} = 1 \quad \forall i \in \mathcal{N}_{comp}(k)$$

$$\sum_{i=1}^{N_{comp}} \theta_{ij} = \mathcal{N}_{comp}(k) \tilde{\mathbf{x}}'_j \quad \forall j \in 3N_s$$

where $\mathcal{N}_{comp}(k)$ is the number of compromised EVs and $\tilde{\pi}_i(j | S, P)$ is the assigned weight of EV i transition to state at index j , given its measurements.

5) **State Index to Measurement Mapping:** Once the optimal state assignment θ_i is determined for each compromised vehicle i , the final step maps this abstract assignment to concrete manipulated measurements ($\tilde{S}'_i, \tilde{P}'_i$). The one-hot vector θ_i , where $\theta_{ij} = 1$, identifies the target state index j for the next time step, defining the new operating mode (e.g., Charging, Discharging, or Idle) and the corresponding SoC range.

$$\tilde{P}'_i : \begin{cases} 0 & \text{if CM} \rightarrow \text{IM} \\ 0 & \text{if DM} \rightarrow \text{IM} \end{cases} \quad \tilde{P}'_i : \begin{cases} P_{d,i} & \text{if IM} \rightarrow \text{DM} \\ P_{c,i} & \text{if IM} \rightarrow \text{CM} \end{cases} \quad (15)$$

$$\tilde{S}'_i = \tilde{S}_i + \text{sgn}(\tilde{P}'_i) \cdot \left\lceil \frac{|\tilde{P}'_i \cdot T_p|}{Q_i} \right\rceil \quad (16)$$

This process ensures that the generated measurements ($\tilde{S}'_i, \tilde{P}'_i$) are consistent with the vehicle's physical capabilities and adhere to the stealthy conditions in (7) and (8).

6) **Update IEVM with Manipulated Measurements:** All manipulated measurements are used to update the IEVM, which will be used in the next attack optimization interval.

7) **IEVM's Transmission of Manipulated Measurements:** Updated simulation measurements of compromised EVs are sent to the operator.

8) **eSSM Construction:** To construct its eSSM model, the operator utilizes the most recent EV measurements, which consist of both true (S_i, P_i) and manipulated ($\tilde{S}'_i, \tilde{P}'_i$) values.

IV. NUMERICAL VALIDATION

This section details the numerical validation of the proposed stealthy FDIA, quantifying its impact on V2G system operations, including grid flexibility estimation and frequency stability. Simulations were conducted with Python and MATLAB.

The simulation setup involves a fleet size of 10,000 EVs, with their comprehensive specifications detailed in Tables I [10]. The utility's eSSM utilizes 10% SoC interval discretization. To simulate a realistic attack scenario, a random 30% of the connected EVs are designated as compromised at the simulation's onset. These compromised EVs are then subject to the attacker's manipulation of their reported measurements immediately after sending their initial connection signal to the operator.

A. FDIA with No Control

In this scenario, the operator solely utilizes the eSSM to estimate the grid's inherent flexibility, without actively dispatching control signals. As demonstrated in Fig. 5, upon

attack initiation at 12:00, the eSSM's estimated grid flexibility gradually diverges from its true value. The marked overestimation of the upper bound of the eSSM's flexibility is a direct consequence of the compromised EVs being manipulated to continually report their mode as charging, thereby inflating the perceived available power for grid services. This section highlights the attacker's ability to create a persistent illusion of greater grid support.

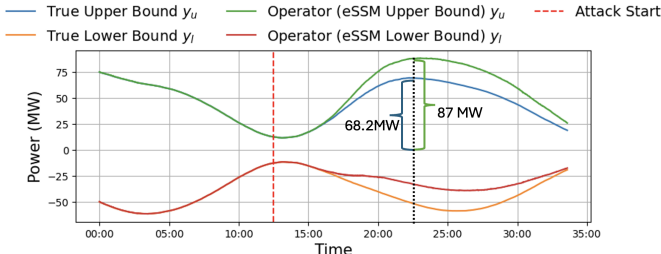


Fig. 5: Grid Flexibility with No Control. Upper and lower bounds of EVs' flexibility from SSM under attack are represented as y_u and y_l , respectively.

B. FDIA with Control

This subsection evaluates the attack's efficacy when the utility actively employs the eSSM for frequency regulation within secondary frequency control under a closed-loop framework. As depicted in Fig. 2 and described in Section II, the operator generates control signals based on its eSSM to meet dispatch requests.

The attacker manipulates the compromised EV measurements, causing the operator to perceive the aggregated state distribution as (13). Consequently, the operator broadcasts faulty control signals intended to adjust the EVs' state indices. However, since the EVs' true measurements (P_i, S_i) are unaltered, they disregard these control signals, which do not correspond to their actual state indices. As illustrated in Fig. 6, this discrepancy results in a substantial degradation in power correction accuracy.

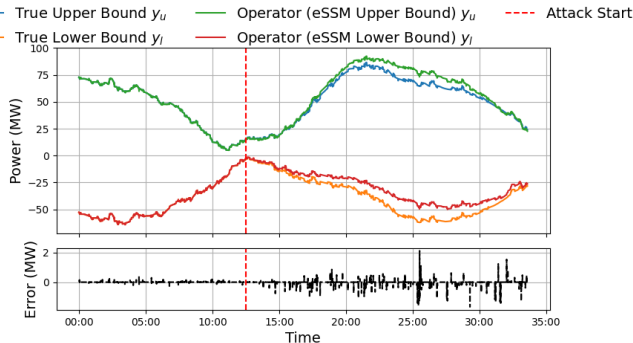


Fig. 6: Grid Flexibility with Control

Quantitatively, the attack leads to a dramatic increase in the Mean Absolute Percent Error (MAPE) of power correction. The pre-attack MAPE of 5.49% surges to 520.28% during the attack period. This significant increase demonstrates the attack's success in undermining the operator's capacity to accurately manage grid services. This would directly translate into severe operational inefficiencies, substantial economic losses, and critically compromise the reliability and stability of the grid.

TABLE II: AGC Parameters

Parameters	H_i	D_i	R_i	T_{gi}	T_{Ti}	K_{ai}	B_i
Area 1	10	0.6	0.05	0.2	0.5	0.3	20.6
Area 2	8	0.9	0.0625	0.3	0.6	0.3	16.9
$K_T = 2$	Base Power = 400 MVA						

C. AGC Simulation

To illustrate the critical real-world implications of the misestimated flexibility, a 2-area AGC system was simulated using Simulink. The AGC system as shown in Fig. 7 and parameters are detailed in Table II. Both generators are configured to have a maximum operating point of 200 MW, while the base load on both areas is $P_L = 0.475$ p.u. The operator in Area 1 possesses the V2G capability and can perform power corrections by dispatching control signals.

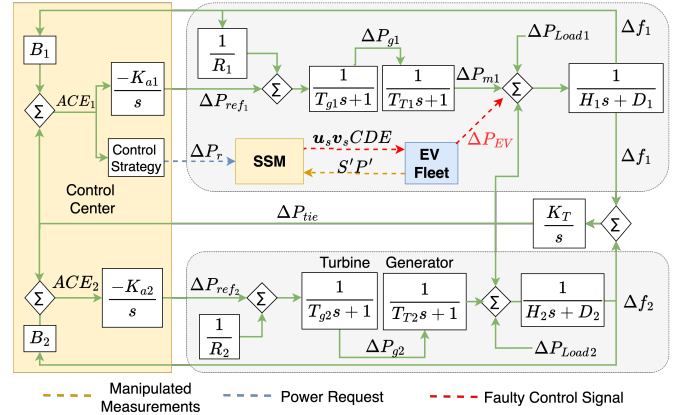


Fig. 7: 2-Area AGC Simulation With Aggregated EV Model

A predefined control strategy is implemented, designed to receive the Area Control Error (ACE) and determine the requisite power change (ΔP_r) for frequency correction. We simulated a case where the power demand in Area 1 sharply increases by 50 MW at 22:00 (bounds of the grid flexibility as shown in Fig. 5), represented by a step function ΔP_{L1} . Given that the conventional generators are unable to compensate for this demand entirely, the control center dispatches $\Delta P_r = 50$ MW to the EV operator.

The true upper bound of grid flexibility (Fig. 5), denoted as y_u (measured at 68.2 MW), is technically sufficient to satisfy the utility's power request (50 MW). However, the EV operator generates the control signals based on a manipulated aggregated state, \tilde{x}' . The construction of these control signals relies on a priority function (detailed in Section II), which is fundamentally driven by the aggregated state distribution. Consequently, any significant deviation in this distribution leads to the generation of faulty control signals. In the event described, the EVs intended for state-switching are not located within the presumed aggregated states. As a result, the targeted EVs discard the received signals because they are deemed non-applicable, leading to a substantial reduction in performance. Therefore, the actual power contribution delivered by the fleet, ΔP_{EV} , is only 25.95 MW.

The mismatch between perceived and actual supply leads to a critical demand-supply imbalance of 4.05MW. As a direct consequence, the power flow over the tie line increases to provide emergency support to the affected area, and subsequently, significant frequency deviations are observed in both areas, as represented in Fig. 8.

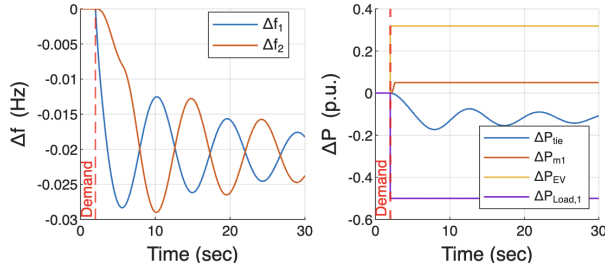


Fig. 8: Impact of FDIA on Δf and ΔP at 22:00 based on the flexibility shown in Fig. 5. ΔP_{EV} is dispatched 100 ms after the load increase. Negative ΔP_{tie} indicates the direction of the power flow (Area-2 to Area-1).

V. CONCLUSION

This paper proposed a novel stealthy FDIA model targeting V2G coordination based on eSSM. Under the realistic assumption of a limited adversary capable of compromising only a subset of EVs, the proposed attack demonstrates how manipulated State of Charge (SoC) and power measurements can deceive the operator's flexibility estimation while remaining consistent with eSSM expectations. Simulation results revealed that the proposed FDIA can significantly distort the perceived flexibility, leading to incorrect control actions and degraded frequency stability, even without direct access to the control infrastructure. These findings reveal that even a partial, stealthy compromise of EV data can lead to severe operational impacts, underscoring the urgent need for robust anomaly detection and defense strategies in future V2G deployments.

Future work will focus on developing dynamic, feedback-aware attack and detection models, along with resilient state estimation mechanisms capable of identifying stealthy, coordinated data manipulation within large-scale, aggregated V2G frameworks.

VI. APPENDIX

Algorithm 1: Transition Weights $\pi(S, P)$

```

1  $\beta_j \leftarrow 0.8(1 - j^2/100)$ ;  $\beta'_j \leftarrow 0.8 - \beta_j$ ,  $\forall j \in \{1, \dots, N_s\}$ ;
2 for  $i = 0$  to  $N_{comp}$  do
3    $w_{stay} \leftarrow 0.8$ ;  $w_{D(own)}$ ,  $w_{U(p)}$ ,  $w_{R(ight)}$ ,  $w_{L(eft)} \leftarrow 0$ ;
4    $SoC_{loc} \leftarrow \text{mod}(S, N_s)$ ;  $j^* \leftarrow f(S, P)$ ;
5   if  $j^* > 3N_s$  then
6      $\lfloor$  // Continue
7   if  $P > 0$  then
8      $w_U \leftarrow \beta'_{j^*}$ ;
9     if  $SoC_{loc} \geq 0.9$  then
10       $w_R \leftarrow 0.9$ ;
11   else if  $P = 0$  then
12      $w_D \leftarrow \beta_{j^*}$ ;
13     if  $SoC_{loc} \geq 0.9$  then
14        $w_R \leftarrow 0.2$ ;
15     else if  $SoC_{loc} \leq 0.1$  then
16        $w_L \leftarrow 0.2$ ;
17   else if  $P < 0$  then
18      $w_D \leftarrow \beta_{j^*}$ ;
19     if  $SoC_{loc} \leq 0.1$  then
20        $w_L \leftarrow 0.9$ ;
21    $\mathbf{w}_{raw} \leftarrow [w_{stay}, w_D, w_U, w_R, w_L]$ ;
22    $\pi_i \leftarrow \sigma(\mathbf{w}_{raw})_i$ ;

```

Algorithm 1 is employed to assign state index transition weights to each compromised and connected EV N_{comp}

according to their SoC and power measurements. As depicted in Fig. 1, EVs state index transition are limited to their neighboring indexes thus, all possible transition stay, right, left, up, down are assigned with a weight (w_{stay} , w_R , w_L , w_U , w_D), while invalid state transition weights are set to zero. The resulting raw weights, denoted $\mathbf{w}_{raw} \in \mathbb{R}^{3N_s}$, are values ties to each available state index transition. These values are then normalized with *softmax* function $\sigma(\mathbf{w})_i = \frac{e^{w_i}}{\sum_{j=1}^{N_{comp}} e^{w_j}}$ for each EV i to convert arbitrary transition weights to probability distribution. Assume j^* is the current state index of the EV.

Except the special states $j^* > 3N_s$ (explained in II-B), all states indexes are assigned multiple transition weights, allowing the attacker to manipulate EVs state index by changing their measurements. As explained in section III-B4, while weights for transitions across operating modes are determined according to EV's SoC interval (β_j and β'_j), transitions within an operating mode are determined by EV's local SoC position (SoC_{loc}).

- β : DM \rightarrow IM \rightarrow CM: EVs with lower SoC are prioritized to falsely indicate mode switching.
- β' : CM \rightarrow IM: EVs with higher SoC values are assigned higher weights for switching to IM.

REFERENCES

- [1] IEA, "Global ev outlook 2024," Paris, 2024, licence: CC BY 4.0.
- [2] Y. Ma, T. Houghton, A. Cruden, and D. Infield, "Modeling the benefits of vehicle-to-grid technology to a power system," *IEEE Transactions on Power Systems*, vol. 27, no. 2, pp. 1012–1020, 2012.
- [3] S. P. Rao, T. S. Olusegun, P. Ranganathan, U. Kose, and N. Gov-eas, "Vehicle-to-grid technology: Opportunities, challenges, and future prospects for sustainable transportation," *Journal of Energy Storage*, vol. 110, p. 114927, 2025.
- [4] L. Zhang, Y. Liu, L. Hao, X. Zheng, X. Liu, and J. Li, "Multi-objective optimal scheduling strategy of microgrid based on v2g technology," in *2022 12th International Conference on Power and Energy Systems (ICPES)*, 2022, pp. 597–601.
- [5] U. C. Chukwu and S. M. Mahajan, "Real-time management of power systems with v2g facility for smart-grid applications," *IEEE Transactions on Sustainable Energy*, vol. 5, no. 2, pp. 558–566, 2014.
- [6] Y. Yang, W. Wang, J. Qin, M. Wang, Q. Ma, and Y. Zhong, "Review of vehicle to grid integration to support power grid security," *Energy Reports*, vol. 12, pp. 2786–2800, 2024.
- [7] N. Sadeghianpourhamami, J. Deleu, and C. Develder, "Definition and evaluation of model-free coordination of electrical vehicle charging with reinforcement learning," *IEEE Transactions on Smart Grid*, vol. 11, no. 1, pp. 203–214, 2020.
- [8] C. Zhang, R. Sheinberg, S. Narayana Gowda, M. Sherman, A. Ahmadian, and R. Gadh, "A novel large-scale ev charging scheduling algorithm considering v2g and reactive power management based on admn," *Frontiers in Energy Research*, vol. 11, 2023.
- [9] V. R. Chifu, T. Cioara, C. B. Pop, H. G. Rusu, and I. Anghel, "Deep q-learning-based smart scheduling of evs for demand response in smart grids," *Applied Sciences*, vol. 14, no. 4, 2024.
- [10] M. Wang, Y. Mu, F. Li, H. Jia, X. Li, Q. Shi, and T. Jiang, "State space model of aggregated electric vehicles for frequency regulation," *IEEE Transactions on Smart Grid*, vol. 11, no. 2, pp. 981–994, 2020.
- [11] Y. Liu, X. Wang, and G. Joos, "An extended state space model of aggregated electric vehicles for flexibility estimation and power control," 2025, to appear in IEEE Power and Energy Society General Meeting. [Online]. Available: <https://arxiv.org/abs/2503.04714>
- [12] J. Johnson, B. Anderson, B. Wright, J. Quiroz, T. Berg, R. Graves, J. Daley, K. Phan, M. Kunz, R. Pratt, T. Carroll, L. O'Neil, B. Dindlebeck, P. Maloney, J. O'Brien, D. Gotthold, R. Varriale, T. Bohn, and K. Hardy, "Cybersecurity for electric vehicle charging infrastructure," Sandia National Laboratories, Tech. Rep. SAND2022-9315, Jul. 2022.
- [13] I. Skarga-Bandurova, I. Kotsiuba, and T. Biloborodova, "Cyber security of electric vehicle charging infrastructure: Open issues and recommendations," in *2022 IEEE International Conference on Big Data (Big Data)*, 2022, pp. 3099–3106.

- [14] J. Antoun, M. E. Kabir, B. Moussa, R. Atallah, and C. Assi, "A detailed security assessment of the ev charging ecosystem," *IEEE Network*, vol. 34, no. 3, pp. 200–207, 2020.
- [15] N. Bhusal, M. Gautam, and M. Benidris, "Cybersecurity of electric vehicle smart charging management systems," in *2020 52nd North American Power Symposium (NAPS)*, 2021, pp. 1–6.
- [16] D. Elmo, G. Fragkos, J. Johnson, K. Rohde, S. Salinas, and J. Zhang, "Disrupting ev charging sessions and gaining remote code execution with dos, mitm, and code injection exploits using ocpp 1.6," in *2023 Resilience Week (RWS)*, 2023, pp. 1–8.
- [17] S. Dey and M. Khanra, "Cybersecurity of plug-in electric vehicles: Cyberattack detection during charging," *IEEE Transactions on Industrial Electronics*, vol. 68, no. 1, pp. 478–487, 2021.
- [18] S. Acharya, Y. Dvorkin, and R. Karri, "Public plug-in electric vehicles + grid data: Is a new cyberattack vector viable?" *IEEE Transactions on Smart Grid*, vol. 11, no. 6, pp. 5099–5113, 2020.
- [19] M. Wang, Y. Mu, Q. Shi, H. Jia, and F. Li, "Electric vehicle aggregator modeling and control for frequency regulation considering progressive state recovery," *IEEE Transactions on Smart Grid*, vol. 11, no. 5, pp. 4176–4189, 2020.